# High and Ultra-High resolution processing of satellite Sea Surface Temperature data over Southern European Seas in the framework of MyOcean project

B.Buongiorno Nardelli[1,2], C.Tronconi[1], A. Pisano[1], R.Santoleri[1]

[1]CNR – Istituto di Scienze dell'Atmosfera e del Clima-Gruppo Oceanografia da Satellite-Roma

[2] CNR – Istituto per l'Ambiente Marino Costiero - Napoli

In the framework of the GMES (Global Monitoring for Environment and Security) MyOcean projects, funded by the European Commission, different remotely-sensed Sea Surface Temperature (SST) supercollated (L3S) and interpolated (L4) data are produced and distributed in near-real time by the Consiglio Nazionale delle Ricerche - Istituto di Scienze dell'Atmosfera e del Clima - Gruppo di Oceanografia da Satellite (CNR). These SST products are based on the night-time images collected by the infrared sensors mounted on different satellite platforms and cover the whole Southern European Seas (i.e. the Mediterranean Sea, including the eastern Atlantic Ocean, and the Black Sea). The CNR processing chains include several modules, from the data extraction and preliminary quality control, to cloudy pixel removal and satellite images collating/merging up to L3S. A two-step algorithm finally allows to interpolate SST data at high (HR 1/16°) and ultra-high (UHR 1/100°) spatial resolution. The basic design and the main algorithms used in MyOcean

processing chains are described hereafter. A validation of the HR super-collating procedure developed during MyOcean is presented. The Mediterranean HR and UHR L3S and L4 operational products have then been validated vs in situ SST measurements from drifting buoys, covering two years of data (2010-2011). The validation includes a comparison between the UHR CNR L4 and the G1SST L4 developed by Chao et al. (2009).

## 1. INTRODUCTION

Several operational and scientific activities related to the retrieval and dissemination of the Sea Surface Temperature (SST) estimates from satellite data have been conducted by the CNR (Consiglio Nazionale delle Ricerche, Istituto di Scienze dell'Atmosfera e del Clima - Gruppo di Oceanografia da Satellite) in recent years (Buongiorno Nardelli et al., 2003; Buongiorno Nardelli and Santoleri, 2005; Marullo et al., 2007; Buongiorno Nardelli et al., 2010;). CNR research and development activities were initiated primarily during three international projects: Medspiration (European contribution to the Global Ocean Data Assimilation Experiment (GODAE) Gridded High Resolution Sea Surface Temperature Pilot Project (GHRSST-PP), funded by the European Space Agency), MFSTEP (Mediterranean Forecasting System: Toward an Environmental Prediction, EU-MAST Project) and MERSEA (Marine EnviRonment and Security for the European Area, EU integrated project), and are now continuing in the framework of important international initiatives: the two European MyOcean projects, and the GHRSST (since 2009 the GHRSST-PP was replaced by the Group for High Resolution SST).

MyOcean-1 implemented the European GMES Marine Core Service (Global Monitoring for Environment and Security) for the 2009-2012 period, and developed the first concerted and

integrated pan-European capacity for ocean monitoring and forecasting. These activities will continue under the MyOcean-2 umbrella in the 2012-2014 period.

GHRSST is an international scientific and technical network specifically set up to address the need for high resolution SST estimates and reliable operational SST products, keeping in mind the requests of several different kinds of scientific, institutional, public and private users (Donlon et al., 2005). GHRSST represents a common framework for the scientific investigation of a fundamental variable that needs to be accurately estimated in order to define and predict the ocean and atmosphere dynamics and climate. In fact, an accurate estimate of the SST is primarily required by the meteorological and marine operational forecasting systems to constrain their numerical prediction models. However, an increasing number of private companies (working, for example, on fisheries, tourism, marine transportation, marine environment and security managing, offshore exploration and extraction, etc.) is also requesting now operational access to SST data.

The main results and recommendations of GHRSST have been reflected in the design of the MyOcean sub-systems devoted to the development and production of satellite SST data (SST-TAC, Thematic Assembly Centre during MyOcean-1 and OSI-TAC, Ocean and Sea Ice Thematic Assembly Centre during MyOcean-2). Within the SST-TAC/OSI-TAC, CNR has the responsibility of developing, implementing and maintaining the operational chains for the production, validation and dissemination of the multi-sensor SST Level 3 data (more precisely L3S data, see GHRSST Science Team, (2010) for a definition of satellite product level) and Level 4 (L4) products covering the Southern European Seas (Mediterranean and Black Sea). The L3S and L4 data are built from all available GHRSST L2P infrared measurements (which include the SST measurements on the original swath and some ancillary information), and correspond to daily (night-time) gridded super-collated (multi-sensor) and optimally interpolated satellite SST estimates at High spatial Resolution (HR) and Ultra-High spatial Resolution (UHR), i.e. at 1/16° and 1/100°, respectively.

The choice of developing interpolated satellite SST products up to ~1 km resolution (1/100°) was driven by user requests. However, the effective resolution of L4 products (mainly at UHR, but

79 also at HR) is limited by the combination of the low number of high resolution cloud-free
80 measurements generally available and of the short time SST response to the processes that drive the
81 ocean surface dynamics, which make UHR space-time interpolation quite difficult (e.g. sub-
82 mesoscale processes, localized air-sea interactions in coastal areas, etc.). Moreover, as thoroughly
83 discussed by Reynolds and Chelton (2010), it is the choice of the analysis procedures and
84 configurations (e.g. weighting functions and background fields), much more than the grid spacing,
85 that determines the true resolution of a L4 product. Consequently, even if the CNR analysis system
86 runs a two-step (two-scale) Optimal Interpolation (OI) algorithm, with different background fields
87 and correlation scales at HR and UHR (as detailed in section 3.4), it is not expected to be able to
88 retrieve UHR features when no observations are present nearby in space and time.
89 A similar multi-scale approach has been proposed and implemented by Chao et al. 2009, who
90 developed a daily, global Sea Surface Temperature (SST) L4 data set at 1 km (G1SST). In order to
91 combine GHRSST L2P data at various spatial resolutions, they applied a two-dimensional
92 variational (MS-2DVAR) blending algorithm. To our knowledge, this is the only other operational
93 SST L4 product reaching 1 km resolution and will thus serve in the following as a basis for the
94 validation of our UHR products.
95 In this paper, the second version (V2) of the CNR MyOcean SST processing chain is presented.
96 The data used for the generation and validation of the products and the core modules of the
97 processing chain are briefly introduced, together with a description of the algorithms for the
98 merging/collating of satellite passes and of the OI technique adopted. A specific section is dedicated
99 to the scientific validation of the HR merging technique that was developed during the first year of
100 MyOcean. This validation was performed comparing the first version (V1) and the V2 L3S products
101 with in situ SST measurements (creating a match-up database with drifting buoy data) and covers
102 one year of data (2008). Successively, all operational L3S and L4 Mediterranean products have
103 been validated vs in situ measurements, concentrating on years 2010 and 2011. As part of the
104 validation, a comparison between UHR CNR L4 and G1SST L4 accuracy is presented.

105 Unfortunately, the extremely low number of in situ measurements covering the Black Sea made it
106 impossible to provide a similar validation for the Black Sea products.
107 All data described hereafter are operationally produced since the beginning of 2010, while L3S
108 products have been operationally released to the public at the beginning of 2012.
109

110 ## 2. DATASETS

111

112 ### 2.1 Satellite observations

113 While a combination of satellite and in situ measurements has been successfully used as input
114 data for some global analyses of the SST (e.g. Reynolds et al., 2007; Donlon et al., 2011), CNR
115 SST system only ingests satellite data. This choice was fundamentally due to the small amount of in
116 situ data available in NRT over the Southern European Seas, and to guarantee the possibility to
117 have a fully independent dataset for validation purposes. More precisely, CNR processing chain is
118 based on the night-time images acquired by the infrared sensors flying on both geostationary and
119 polar orbit satellites. Microwave data are not ingested due to their low resolution and limited
120 coverage of the semi-enclosed Mediterranean and Black Sea basins, caused by land contamination.
121 The sensors (and platforms) ingested in CNR system thus include: the Advanced Along Track
122 Scanning Radiometer [1](AATSR, installed on the European ENVIronment SATellite, ENVISAT),
123 MODerate resolution Imaging Spectroradiometer (MODIS, on both Aqua and Terra satellites),
124 Advanced Very High Resolution Radiometer (AVHRR, on METeorological Operational satellite,
125 METOP, and National Oceanic and Atmospheric Administration (NOAA) satellites), Spinning
126 Enhanced Visible and Infrared Imager (SEVIRI, installed on Meteosat Second Generation, MSG).
127 Corresponding datasets and characteristics are reported in table 1. Additional information on each
128 dataset can be found in *www.ghrsst.org*.

[1]Only until satellite communication failure, occurred on 8th April 2012.

129 The raw data are collected and processed up to the Level 2 (L2, i.e. as SST values retrieved on
130 the native sensor grid/swath) by several different institutions, and are disseminated in a single
131 common format through the GHRSST Global and Regional Data Assembly Centres (GDAC,
132 RDAC; see *www.ghrsst.org* for more details). The GHRSST L2 data are written as netCDF files
133 and contain SST observations, geo-location data, error estimates (SSES, Single Sensor Error
134 Statistics, i.e. bias error and standard deviation error), land and ice flags, as well as additional
135 auxiliary fields for each pixel, referred to as dynamic flags (these files are called L2P data). In
136 particular, L2P dynamic flags include estimates of the surface wind field (that could be used to
137 identify areas potentially subjected to intense diurnal variations), surface solar irradiance (SSI),
138 aerosol optical depth (useful to flag areas contaminated by atmospheric dust) and sea ice
139 concentration (see Donlon and the GHRSST-PP Science Team, 2005, and GHRSST Science Team,
140 2010). Through the Master Metadata Repository (MMR) system, GHRSST also distributes
141 metadata records for each satellite pass, providing information on the single L2P file content
142 (coverage, acquisition time, etc.). This information is used in CNR system for a pre-selection of the
143 files that will be ingested in the processing chain.
144
145 **2.2 In situ measurements and matchup data**
146 In situ SST data collected by surface drifting buoys have been used for the validation of the SST
147 products. The data used in this work are distributed via the GTS (Global Telecommunication
148 System) and have been obtained from two different sources, depending on the period considered:
149 2008 data were obtained from the Canada's Integrated Science Data Management Centre, which
150 provides an archive of all drifting buoy data on behalf of the DBCP (Data Buoy Cooperation Panel)
151 and JCOMM (Joint WMO-IOC Technical Commission for Oceanography and Marine
152 Meteorology), while the 2010-2011 operational data were taken from the MyOcean In Situ
153 Thematic Assembly Centre (In Situ-TAC). The information on the quality of the data has been used
154 to exclude suspect measurements, keeping only the highest quality data (for more details on the QC

155 procedures adopted by the data producers see also Hansen and Poulain (1996), the MyOcean In Situ
156 TAC Product User Manual, http://www.coriolis.eu.org/content/download/5682/42222/file/MYO-
157 INS-PUM-001-V1.pdf, and the quality control guidelines by the DBPC
158 http://www.jcommops.org/dbcp/data/qc.html). Moreover, additional quality control (QC)
159 procedures have been applied to all drifter measurements before building our matchup dataset.
160 These tests include a comparison with a daily pentad climatological SST field (rejecting all values
161 exceeding a difference of 5°C) and with the previous day L4 analysis (rejecting all values exceeding
162 a difference of 1.5°C and only if the reference L4 error is below a fixed value, meaning the previous
163 day analysis effectively includes information coming from valid satellite data and not simply
164 climatological values). Similar QC procedures, especially the climatological check, have been
165 implemented in all MyOcean SST-TAC production units (e.g. Donlon et al., 2011). To evaluate the
166 QC algorithm performance, some tests have been performed (on L3S UHR data), comparing our
167 results with those obtained from other two approaches. As a first test, the fixed threshold check with
168 respect to the previous day L4 was substituted with a standard outlier detection algorithm
169 (iteratively flagging values exceeding 3 or 4 times the standard deviation error). Finally, the Mean
170 Bias Error (MBE) and STandard Deviation Error (STDE) have been computed after applying the
171 black list of malfunctioning drifters as provided by CMS/Meteo-France
172 (ftp://ftp.ifremer.fr/ifremer/cersat/projects/myocean/sst-tac/insitu/blacklist/) in the framework of the
173 MyOcean TAC.

174 The STDE estimated with the iterative flagging procedures were found to be always lower (of
175 about 0.05-0.1°C) than those computed with the fixed threshold, while the black list lead to slightly
176 higher (approx. 0.1 °C) values, even if direct inspection of the matchup data evidenced differences
177 between buoy measurements and corresponding climatological values of more than 5°C, which
178 seem to indicate that the black list is not effectively flagging all malfunctioning drifters at the right
179 time. Even if the check with the previous day L4 analysis might seem to reduce the error artificially,
180 in practice it assumes that local variations (at pixel level) between consecutive nights of more than

181 1.5°C are not physically justified, but rather due to an improper functioning of the in situ sensors. A
182 similar threshold of 1.5°C was fixed after specific tests conducted during MERSEA project by
183 Marullo et al. (2007) to flag residual cloudy pixel in the input L3S data (see also section 3.4.3).
184 A matchup database between L3S and L4 products and surface drifting buoys quality-controlled
185 measurements has thus been compiled. The matchup has been restricted to night-time data (drifter
186 data are searched in the interval between 9 p.m. and 6 a.m.), keeping only one value per buoy for
187 each date, in order to reduce the errors on the drifter measurements and ensure the matchup dataset
188 is made up of fully independent measurements (sequential measurements from the same drifter
189 would give autocorrelated information within the time period considered, see also Bayley and
190 Hammersley, 1946). Actually, the drifting buoys collect SST data at regular time intervals (based
191 on an internal clock), while position measurements are recorded at longer time intervals, according
192 to the satellite positioning system. The single SST value per buoy/day used here is thus the one
193 collected closest (in time) to the position time and closest (in time) to the nominal interpolation time
194 (00:00 UTC). Finally, the matchups were built by taking the satellite SST value of the pixel
195 corresponding to the selected drifter position.
196

197 ## 3. PROCESSING CHAIN

198

199 The CNR SST processing chain consists of two main sequential sub-chains: the HR processing
200 (that is run first), and the UHR interpolation. This architecture was designed as a consequence of
201 the specific algorithm used for the UHR interpolation (see section 3.5). The whole processing is
202 organized in six main modules/packages (M1-6), which are governed through a specific System
203 Controller (see the scheme in figure 1). The System Controller manages the sequence of operations
204 and includes all error handling and communication procedures, processor logging, as well as the
205 internal and external interfaces monitoring. These modules can be considered as ‘logical’ steps that

206 are executed by both the HR and the UHR chains, while the specific software modules have
207 necessarily been adapted or configured to run differently when called by one processing or by the
208 other. All packages allow an easy configuration of the main parameters required by each operation
209 through configuration files. The functionalities of the first four modules are described in the
210 following, together with a presentation of the main theoretical and practical issues related to the
211 processing, in particular for what concerns the sensor bias adjustment and the interpolation of the
212 SST data.
213
214 **3.1 External data collection (M1)**
215 This module drives the external interface from the input data providers to the internal input data
216 archive. It includes configurable connection protocols and editable lists of the sensors to be
217 considered (such as those listed in table 1). It collects the L2P metadata from GHRSST GDAC and
218 RDAC and uses them to select and download only the L2P data covering at least part of the
219 interpolation areas. This module is unique for both HR and UHR, and it is activated at regular time
220 intervals (every three hours). Specific messages are sent to the system manager to warn about
221 missing input data.
222
223 **3.2 L2P data extraction, preliminary data quality control and remap to L3 (M2)**
224 The second module performs the L2P data pre-processing to L3P. Single sensor/single image SST
225 data are first extracted based on the geographical coverage and local time of the observations.
226 Present configuration only selects the observations collected between 9 p.m. and 6 a.m. (local pixel
227 time), in order to avoid diurnal warming contamination (see also Buongiorno Nardelli et al., 2005,
228 Marullo et al. 2010). A quality control of the L2P data is applied, based on the quality flags and
229 confidence values associated to each pixel by the data providers (the same quality levels are defined
230 for all sensors, see also Donlon and the GHRSST-PP Science Team (2005) and GHRSST Science
231 Team (2010) for a detailed description of the quality levels computation). All the threshold

parameters used at this stage can be configured through a configuration file. Presently, only the data marked with the highest quality level are processed. Selected valid data are then remapped over the L3S/L4 interpolation grids (at both HR and UHR resolution). The remapping is performed computing a weighted average of the L2P observations found within the final L3P/L4 grid cell (the weights being given by the inverse of the distance to the centre of the cell, e.g. with Shepard's method). The procedure essentially selects the nearest neighbour if the final grid resolution is comparable to the input grid one (e.g. in the UHR case or when considering SEVIRI data in the HR processing). The Mediterranean HR grid corresponds to the first level of the MyOcean Mediterranean Modelling and Forcasting Centre (MFC) 1/16° grid. A similar grid has been generated for the Black sea (at 1/16°).

All UHR grids have been derived from the global land/sea tag file provided by NAVOCEANO (https://www.ghrsst.org/data/ghrsst-data-tools/navo-ghrsst-pp-land-sea-mask/).

### 3.3 Sensor bias adjustment: background

While it is sometimes believed that a direct combination of multiple L3 observations (with different accuracy levels) within an OI algorithm might produce a more accurate SST estimate, there are a number of theoretical and practical reasons to apply a preliminary bias adjustment procedure and a successive collation of L3 data before interpolating them.

First of all, only if the observation errors are purely random and a sufficient number of observations are available, they can be reduced by averaging. Conversely, systematic errors will not be revealed just by looking at repeated measurements by the same sensor or eliminated by averaging different sensors' measurements, especially if the number of available sensors is quite small (see also Rabinovich, 2000). As discussed below, spatially correlated errors found in satellite images can often be related to systematic errors, and a specific treatment of these errors is thus of fundamental importance.

More precisely, the SST estimated from one sensor might significantly and systematically differ from that retrieved by another sensor under the same conditions, both as a consequence of the differences among the sensors themselves (number of bands, spectral resolution, scanning/viewing geometry, etc.) and/or of the different retrieval algorithms applied (see also Høyer et al., 2012). These latter, in particular, might correct very differently the atmospheric contribution to the measured brightness temperature, possibly leading to systematic errors (e.g. a sensor/algorithm constantly underestimating the SST in the presence of aerosols, e.g. Pathfinder SST, Xu and Ignatov, 2010).

Rapid changes in the atmospheric conditions and uncertainties in the correction algorithms might then lead to spatially correlated biases at large spatial scales, even between images acquired by the same sensor at different times of the day. These errors will generally lead to a slightly higher standard deviation when evaluating L2P SSES (which are computed from long time series of matchup data, thus spanning many possible conditions), even though resulting in low mean biases. Then, SSES biases cannot be considered strictly representative of the errors in a single image, and simply averaging the different images will not necessarily improve the accuracy. On the contrary, all observations need to be accurately inter-calibrated before entering an OI procedure.

In fact, as an additional limitation, the occurrence of large scale (spatially correlated) biases in single images makes the application of OI (OI) algorithms inefficient, as standard OI requires the errors in the observations to be uncorrelated (e.g. Bretherton et al. 1976). Consequently, an appropriate combination of multiple data points through OI cannot be performed unless spatially correlated errors are removed.

The bias correction thus represents one of the most difficult and crucial steps in the SST data processing, as it directly influences the quality of the final product. Different strategies have been proposed to correct sensor biases until now, the majority of which are based on the adjustment of the single sensor to a reference sensor. As an example, the adjustment performed within the Operational SST and Sea Ice Analysis system (OSTIA, see Donlon et al., 2011) is obtained by

283 running an OI on each sensor bias field, as retrieved by comparing each sensor to AATSR, whose
284 accuracy resulted to be comparable, if not better than, to that of in situ measurements (O'Carrol et
285 al., 2008). This first analysis is run with correlation length scales of 700 km, representing the typical
286 e-folding scale of synoptic weather patterns.
287 Similarly, the bias correction applied at the Ocean and Sea Ice–Satellite Archiving Facility (OSI-
288 SAF) is based on a daily analysis of the differences between a given sensor and the AATSR over
289 the previous 5-10 days, on a 5°×5° grid. The correction is then obtained by spatially and temporally
290 averaging the differences (Le Borgne et al., 2011). On the other hand, different approaches to the
291 satellite bias adjustment have been proposed by Reynolds (1988) and Reynolds et al. (2007). Both
292 are based on the combination of in situ and satellite data and either on the solution of a Poisson
293 equation (which adjusts satellite data to in situ measurements by imposing in situ measurements as
294 internal boundary conditions), or on the analysis of the Empirical Orthogonal Teleconnection (EOT)
295 of in situ and satellite SST anomalies.
296
297
298 **3.4 Sensor bias adjustment, L3 super-collating and additional cloud screening at CNR (M3)**
299
300 Two different algorithms for the sensor bias adjustment and data super-collating are used in
301 CNR HR and UHR processing chains. Super-collation is easier at HR than at UHR because some
302 small scale merging artefacts that might occur at UHR are effectively removed by the HR binning.
303
304 *3.4.1 Bias adjustment and super-collating algorithm at HR resolution*
305 The HR scheme has been originally developed within MERSEA, but it was significantly
306 optimized during the first year of MyOcean-1 Project.
307 While it would be possible to build super-observations by combining/averaging the
308 measurements from all different sensors at each grid point (e.g. through a simplified optimum

309 averaging of single sensors super-obs., as in Reynolds et al. 2007), our scheme builds a single
310 super-collated image per day by selecting only the highest quality measure available for each grid
311 point. This choice is basically due to computational limitations and timeliness requirements of the
312 operational chain, which make the ingestion of all single adjusted L3P measurements unfeasible.
313 Consequently, our system is now ingesting a single value of adjusted SST per grid point for each of
314 the days within the temporal window considered.

315 The measurement quality is defined through a pre-determined sensor validation statistics, and a
316 simple hierarchy of sensors is identified coherently (see table 1). This hierarchy is based on the
317 validation statistics computed in the framework of the MyOcean CAL/VAL activities
318 (http://projets.ifremer.fr/cersat/Data/Quality-control/MyOcean-SST-QC/Control-Validation-
319 MyOcean/L2P-In-situ) and it is eventually updated in the operational chain at the end of each
320 MyOcean phase (i.e. approximately every year during MyOcean-1 and quarterly during MyOcean-
321 2). As a preliminary step, the single image bias is estimated and removed through an iteratively
322 updated reference as described below.

323 In practice, sensors whose SST values do not need to be corrected (e.g. the AATSR) are included
324 in a reference sensor list, and corresponding data provide an initial reference SST map. Similarly, a
325 list of sensors to be adjusted is defined. In this second list, sensors that have a better accuracy are
326 placed first, and lower accuracy sensors come last (i.e. they are sorted with decreasing accuracy). At
327 each step, the processing ingests a new sensor image searching it sequentially from this second list.
328 For each pixel, only the first observation found is retained (thus only the measurement from the best
329 sensor available is considered at each location). However, before adding any new data to the
330 merged map, eventual large scale biases between each image and the reference map (i.e. the pixels
331 that have already been merged) are estimated and removed. The merged SST map is thus updated
332 every time a new valid observation comes in, and it is then used as reference for the successive step.

333 In the original CNR algorithm (V1), the bias was estimated at each of the steps described above
334 from the overlapping areas between each new image and the reference map, and a single correction

was then applied to the whole image. On the contrary, the V2 algorithm was specifically designed to apply a smoother bias correction (i.e. a correction that doesn't create artefacts or spurious gradients at image edges). This algorithm does not differ much from the OSTIA approach (Donlon et al. 2011), except for the method used here to interpolate the single image biases and for the iteratively updated reference used. In practice, an initial bias correction map is estimated by subtracting the reference sensor values to the uncorrected observations. This map will display valid data only where the images overlap, while it is filled by NaN (Not a Number) values elsewhere. The bias is then set to zero in the pixels where an estimate of the SST difference is not present and that are at a distance of at least 1500 km from the overlap zones. The successive step is the iteration (100 cycles) of a 10-grid point moving window average (which ignores NaN values), which thus smoothly interpolates the bias correction from the available SST difference towards the areas set to zero. At each iteration, the bias correction is set back to the first iteration values where it originally contained valid numbers (namely, at the pixels that contained valid SST difference values or that were set to zero). The validation of this algorithm is described in section 4.

*3.4.2 Bias adjustment and super-collating algorithm at UHR resolution*

The procedures applied at 1/16° resolution may lead to spurious SST gradients at UHR resolution, in case of uneven distribution of data and/or if small scale scattered clouds are present in the higher accuracy sensor images. This means that selecting data from a high accuracy sensor (as defined in the HR super-collating algorithm) might not be the best option if the source image is 'spotty', as the super-collated image might then display artificial gradients at the spots' edges. As a consequence, UHR scheme is based on a different bias adjustment procedure and sensor hierarchy, even if, similarly to the HR, also the UHR processing builds a single super-collated image per day by selecting only the highest quality measure available for each pixel. The difference is due to the fact that the quality is now defined keeping into account some topological features characterizing each individual image. In fact, the bias is not estimated with an iterative update of the SST

361 reference (as for HR) but computing the difference between each sensor image and a first guess
362 field, that is build directly from the HR L4 SST (see section 3.5). The bias is thus estimated and
363 removed locally (50 km moving bins). The quality of the single adjusted L3P image is then defined
364 taking into account the continuity of the measurements in each image, and the higher quality data
365 are selected based on a measure of corresponding data 'sparseness' (spotty/scattered data being
366 classified with lower quality). Quantitatively, the local data sparseness is estimated as the Euclidean
367 norm of the SST gradient, computed after assigning an unrealistic negative value to non-valid data
368 (e.g. -99). In this way, the gradients are much higher near cloud/image borders, and, for each pixel,
369 the image that displays the lowest gradient is selected as the less sparse data source. Though more
370 sophisticated numerical techniques can be proposed to estimate the gradient, for our purposes it was
371 sufficient to apply a simple centred finite difference method.
372
373 *3.4.3 Additional cloud contamination check*
374 As part of the merging procedure, an additional check on cloud contamination is also performed
375 both at HR and UHR. This check flags the pixels that are colder than the previous day value (by a
376 fixed threshold, now 1.5°C), as measured in the corresponding super-collated L3 (when present).
377
378 **3.5 Space-time OI of L3 data (M4)**
379 The classical OI (OI) method (Gandin, 1965, Bretherton et al., 1976) has been adapted to the
380 Mediterranean and Black Sea MyOcean SST HR and UHR processing, starting from the previous
381 experiences of CNR (Santoleri et al., 1991; Buongiorno Nardelli et al., 2003; Marullo et al., 2007;
382 Buongiorno Nardelli et al., 2010, Marullo et al, 2010). More precisely, the core of the CNR
383 MyOcean HR OI module has been developed in the framework of the MERSEA Integrated Project,
384 while the UHR one has been specifically designed for MyOcean.
385 In practice, the SST L4 analyses are obtained as a linear combination of the observations
386 (namely, of the SST anomalies with respect to a *first guess*), weighted directly with their correlation

387 to the interpolation point and inversely with their cross-correlation and error. OI theory assumes the
388 statistical characteristics of the parameter variability are known (*background error covariance* and
389 *observation error covariance*). While several operational systems are based on purely spatial OI
390 algorithms, using daily innovations as input data (i.e. using previous day analysis as a first guess,
391 and eventually relaxing to a climatology in the absence of new observations, e.g. Donlon et al.,
392 2011, and references therein), CNR scheme directly applies a space-time OI. Different first guess
393 fields, correlation functions, influential data selection criteria and noise to signal ratios are used in
394 the HR and UHR processing as synthesized in table 2. The common HR and UHR features will be
395 only briefly described in this section, while more details will be given on the algorithm built for the
396 UHR interpolation, as HR algorithm has already been fully detailed in Marullo et al. (2007) and
397 Buongiorno Nardelli et al. (2010).

398 The HR statistical interpolation scheme starts from a climatological field (first guess), but the
399 SST measurements collected within the ten days prior to the interpolation day are directly included
400 in the analysis (properly weighted by the space-time correlation function selected). The
401 climatologic field is given by a daily pentad climatology built from 21 years of AVHRR Pathfinder
402 data, as described in Marullo et al. (2007) and Buongiorno Nardelli et al., (2010), for the
403 Mediterranean and Black Sea, respectively. These authors focused on the re-analysis of the
404 Pathfinder data (Kilpatrick et al., 2001) that was performed during MFSTEP and SESAME projects,
405 but they applied exactly the same OI scheme used in the MERSEA/MyOcean HR processing
406 (covariance models, data sub-sampling strategy, inversion technique, etc.).

407 The strategy adopted here to interpolate the SST field at the resolution of ~1 km (UHR) is based
408 on the concept of "scale separation/decomposition". In practice, it is assumed that the SST
409 variability is given by the superposition of processes occurring at different characteristic scales
410 (which do not interact among themselves), and that each scale can thus be interpolated separately,
411 provided a proper filtering is applied. A similar approach is used by the Japan Meteorological

412 Agency (JMA) to obtain their Merged Global Development SST product (Sakaida et al., 2005), as
413 well as by Chao et al. (2009) for their G1SST product.

414 Actually, it may be noticed that the smaller scales (of the order of few km) have already been
415 filtered out in the HR maps, both through binning on the 1/16° resolution grid and through the
416 filtering performed by OI itself, given the spatial and temporal background error correlation scales
417 used. It may then be assumed that the lower resolution map only contains the larger scale signals
418 (i.e. mesoscale, sub-basin features, and larger scales etc.). Consequently, the HR L4, properly re-
419 binned on the UHR grid, may be used as a *first guess* for a second UHR interpolation step. The
420 upsizing of the HR field on the UHR grid is presently performed in the operational chain through a
421 simple bilinear algorithm, but this will be improved in the next future by applying a thin plate spline.
422 The SST anomalies (with respect to the first guess) in input to the OI, estimated now at 1 km, will
423 then contain only the small scale signals (i.e. sub-mesoscale and smaller scales) and some noise,
424 and are assumed independent from the background.

425 In order to reduce the number of operations required by the statistical interpolation (mainly by
426 matrix inversion), for each interpolation point, the observations in input are selected only within a
427 limited sub-domain (within a space-time window). In practice, the L3S data are collected within a
428 temporal influential radius of ten days at HR, and only the measurements from the previous and
429 same day are selected at UHR. Analogously, the spatial influential radius ranges between 300 and
430 900 km at HR and is limited to 20 km at UHR.

431 Both the HR and the UHR schemes then drive multiple analyses on different sub-basins/regions
432 to avoid data propagation across land from one sub-basin to the other, but also to speed up the input
433 data search. In practice, different data search and interpolation grid masks (built cropping the
434 original grid) have been defined, and the scheme is run several times. Different sub-basin grids for
435 the HR processing (eastern Atlantic, Western Mediterranean basin, Tyrrhenian Sea, Adriatic Sea,
436 Levantine basin, Aegean sea, Maramara Sea, Black Sea) and 175 masks for the UHR are used,
437 respectively. Two different grids are used for each sub-basin/mask, one identifying the interpolation

points and one the input data selection area, to avoid artefacts at the border of the different masks. In fact, the latter masks include buffer zones at the borders, whose dimensions are defined by the spatial input data search radius. Before entering the influential data selection within each analysis, L3S images are also checked for residual cloudy pixels at both resolutions. More in detail, a low-quality data margin erosion is applied (basically coinciding with cloud margin), flagging all values within a distance of *m* pixels to a pixel already flagged as 'low-quality'. A further check is then performed through the comparison to the closest (in time) L4 analysis available. However, to reduce the risk of flagging also valid data, this last check is performed only if the previous analysis error is lower than a pre-defined value. In practice, the observations that differ from the reference field for more than a fixed threshold (usually $2\sigma$, where $\sigma$ represents the average standard deviation between consecutive night images =0.7 °C) are not included in the analysis.

Computational time limitations still require a further sub-sampling of selected observations in our OI scheme. The method chosen here aims to obtain a balanced data coverage within the influential space-time radius and it consists of a few steps. Observations are first sorted as a function of their correlation to the interpolation point. The most correlated observation is selected first, while all successive data are selected only if they are found along a new direction in the space-time (until $n=50$ observations are found), this allows to avoid/minimize the use of cross-correlated observations in the dataset used to compute the OI field.

Finally, while the background covariance functions used at HR are those adopted within MERSEA project (namely, a negative exponential with decorrelation scales of 150 km and 7 days), different background covariance scales have been tested at UHR. Even if there are plans to estimate the UHR covariance model directly from observations, it has been presently defined as a result of empirical tests, based on a subjective analysis of the norm of the SST gradient and of the norm of the gradients of the SST daily increment ($\Delta$SST) maps (e.g. looking at the presence of interpolation artefacts). The spatial decorrelation lengths have thus been varied between 5 and 15 km, but very

small differences have been found on the interpolated maps in the whole range considered. The smallest value is currently used in the operational chain. Similarly, the time scale was set to 1 day.

## 4. VALIDATION

Two main validation exercises have been carried out. The first one aims to assess the performance of the MyOcean HR super-collating technique with respect to the previous method applied at CNR. This first part was performed comparing both the HR L3S and L4 data obtained with the two algorithms described in section 3.4.1 with in situ data from surface drifters (section 4.1). This validation is limited to the dataset used for the development of the V2 HR super-collating procedure, thus covering the 2008 data over the Mediterranean Sea.

The second one (Section 4.2) is dedicated to the validation of both the HR and UHR operational products over the Mediterranean Sea (not enough in situ data over the Black Sea are available to provide a significant validation). This second validation covers the years 2010 and 2011.

### 4.1 Validation of the HR super-collating procedure

The validation of the V2 merging/super-collating procedure at HR has been performed on the Mediterranean L3S and L4 products. Different approaches have been chosen to perform the comparison between the CNR V1 and V2 algorithms described in section 3.3.

A first validation has been conducted by analyzing some of the metrics suggested by the GHRSST, i.e. looking at the norms of the SST spatial gradient and SST daily increment (ΔSST) spatial gradient as estimated from the super-collated L3 data. In fact, image bias correction and merging problems usually become more evident when looking at spatial gradient intensity maps, where they usually “pop up” as spurious structures with unrealistic shapes, if not directly appearing as straight lines identifying image borders. Though more sophisticated edge detection methods

could be used (and are often applied to study the presence/evolution of thermal ocean fronts, e.g. Cayula and Cornillon, 1992), in our test the gradient was estimated through a simple central finite difference scheme. For the sake of clarity, a typical example showing problems with the V1 bias correction algorithm is presented in figure 2 and 3. The majority of the features visible in these images are related to hydrodynamic structures (meandering currents, eddies, etc). However, the straight line in the Alboran Sea and the straight line from Tyrrhenian Sea to the Channel of Sicily (highlighted in the images, corresponding with the border of the satellite pass) are clearly not related to any oceanographic structure. Indeed, these fake gradients are completely removed with the V2 processing.

Though a simple visual inspection of the spatial gradients can be used to qualitatively evaluate the performance of the merging algorithms, a quantitative validation can be obtained by comparing the gradient intensity averaged over the whole domain. As shown in figure 4, the V2 algorithm systematically reduces the occurrences of spurious spatial gradients in the ΔSST L3 data, as lower mean values are generally observed.

The relatively low number of drifting buoys measurements collected in 2008 over the Mediterranean Sea and the strict QC checks performed lead to a relatively low number of matchups with L3S data (~1200). These matchups are unevenly distributed spatially, with the majority of the observations in the Atlantic portion of the domain, where most of the in situ drifter data were acquired (see figure 5a-b). A higher number of matchups was obtained when comparing buoys and L4 data (~2900), even though with a similar spatial distribution (figure 5c-d).

The V2 merging procedure improves the SST estimate both in terms of STDE (standard deviation error) and MBE (mean bias error). In particular, while no changes were found on the L3S MBE (-0.03°C), the L4 MBE improved with the V2 algorithm, being reduced from -0.06°C to -0.03°C. The L3S STDE was also reduced from 0.53°C to 0.48°C and the L4 STDE was also slightly improved, from 0.46°C to 0.45°C, when applying the V2 merging procedure (see also figure 6).

514

515 **4.2 Validation of the HR and UHR operational products**

516 The validation of the CNR HR and UHR operational products has been performed only over the
517 Mediterranean Sea, due to the low number of drifting buoy SST measurements available over the
518 Black Sea (see section 2.2). With respect to the computations performed in section 4.1, additional
519 analyses have been carried out here, both based on the matchup with drifter data, covering the
520 period 2010-2011, and comparing the CNR L4 accuracy with respect to G1SST L4. The uneven in
521 situ data coverage (Fig. 7, 8, 12) shows that the validation is significantly biased towards the
522 western regions, with very few drifters available in the Levantine basin.

523 As a first step, the STDE and MBE with respect to in situ data have been computed considering
524 the entire matchup database (2010-2011) with 4902, 3971, 8728 and 9043 matchups for the HR L3S,
525 UHR L3S, HR L4 and UHR L4, respectively (see also figure 9). It has to be noticed that HR L3S
526 includes SEVIRI measurements, so that a higher number of matchup is found with respect to UHR
527 L3S.

528 The STDE is quite similar for the two L3S products, attaining around 0.51°C for the HR and
529 0.53 °C for the UHR. Correspondingly, the MBE was slightly higher for the HR L3S (-0.20°C) than
530 for the UHR L3S (-0.07°C). The difference between these statistics could be due either to the
531 different spatial coverage of the two datasets, either to the lower accuracy of SEVIRI data with
532 respect to UHR sensors or to the bias adjustment procedures themselves. Smaller differences
533 between HR and UHR products have been obtained when comparing in situ and L4 data, with a
534 STDE of about 0.52 °C both in the HR and UHR cases and MBE of about -0.1°C and -0.09°C,
535 respectively. It has to be noticed that the L4 statistics do not change significantly, thus indicating
536 that the interpolation is not introducing significant errors.

537 The validation has then been extended to evaluate how the quality of the products varies with
538 time and in space. In figure 7 and 8, the spatial distribution of the matchup data for the period 2010-
539 2011 is displayed for the L3S and L4 products, respectively, together with the associated

differences between in situ and satellite data (in colour). A clear pattern could not be identified for any of the products considered. Looking at the monthly statistics, reported in figure 10, the first thing to be noticed is a general underestimation of the satellite SST with respect to the in situ measurements, during summer (of the order of a couple of decimals). This difference is compatible to the cool skin effect described in Donlon et al. (2002). All HR data displayed similar behaviours. On the other hand, a significant improvement with respect to the climatological field (see section 3.5) has been recorded in all seasons in both HR and UHR L4 data.

As a final step, we compared our UHR L4 products with the Global 1 km SST (G1SST) data, produced daily by the JPL ROMS (Regional Ocean Modeling System) group. To our knowledge, this is the only other operational SST L4 product reaching 1 km resolution. In order to obtain gap-free SST data at various spatial resolution, they apply a two-dimensional variational (MS-2DVAR) blending algorithm (Chao et al., 2009). The statistics have been computed for the full year 2011, when both CNR products and G1SST L4 data were available, over the Mediterranean Sea. While the statistics computed from our products do not change much with respect to the full validation, it must be stressed that both the STDE and MBE computed from G1SST data display higher values than MyOcean products (namely, 0.64°C vs 0.49°C and 0.12°C vs -0.12°C, figure 11 a-b). The negative bias in CNR products can probably be ascribed to the cool skin effect (not presently corrected in the CNR processing chain). Conversely, both the positive MBE and the higher STDE in the G1SST data are probably related to an incorrect flagging of pixels affected by diurnal warming (mostly in the central and western Mediterranean, see figure 12), as G1SST includes also day-time images, simply flagging the areas where wind speeds are less than 4 $ms^{-1}$. Looking at the monthly statistics (Fig. 13), this seems to be the case especially during April-May-June 2011, where stronger warming events have been registered.

## 5. SUMMARY

The basic design and the main modules of the CNR satellite SST operational processing chain, as implemented in the framework of the European MyOcean projects, have been described in this paper. Particular attention has been paid to the description of the HR and UHR bias correction algorithm and super-collating procedures, as well as to the UHR interpolation scheme developed within MyOcean-1 project. The V2 HR L3S and L4 bias correction algorithms were compared to previous techniques adopted at CNR and validated both by looking at the SST and daily SST increment spatial gradients, and compiling a specific matchup database between satellite estimates and in situ SST measurements (collected by drifting buoys and distributed through GTS). This first validation was performed on the test dataset used in the bias adjustment algorithm development phase, covering year 2008. The results evidenced that the proposed new algorithm is able to remove many of the spurious structures that appeared in the HR SST fields as a consequence of inaccurate large scale bias corrections, and also showed that the errors estimated through the comparison with in situ data were reduced with the V2 super-collating algorithm. The operational HR and UHR SST estimates were then compared with in situ drifting buoy SST measurements and to the G1SST L4 products (Chao et al., 2009) providing a full validation of the MyOcean CNR L3S and L4 products. Though satisfactory results were evidenced by this validation, a number of improvements to the CNR operational chain are planned in the future. The main issues that will be investigated are related to the choice of the first guess and covariance model to be used in the OI.

## 6. ACKNOWLEDGEMTS

We wish to thank dr. Richard Reynolds, Prof. Marvin Bauer and the first anonymous reviewer for their helpful comments and constructive criticism.

588 This work has been carried out in the framework of the MyOcean project (Development and pre-
589 operational validation of GMES Marine Core Services (2009-2012), funded within the call EU FP7-
590 SPACE-2007-1 (Grant Agreement nr. 218812).
591
592

## REFERENCES


Bayley, G. V., & Hammersley, J. M. (1946). The "Effective" Number of Independent Observations in an Autocorrelated Time Series, Supplement to the *Journal of the Royal Statistical Society*, Vol. 8, No. 2, pp.184-197.

Bretherton, F.P., Davis, R.E. & Fandry, C.B. (1976). A technique for objective analysis and design of oceanographic experiments applied to MODE-73. *Deep Sea Res*., 23, 559–582.

Buongiorno Nardelli, B., Larnicol, G., D'Acunzo, E., Santoleri, R., Marullo, S. &. Le Traon, P.Y (2003). Near Real Time SLA and SST products during 2-years of MFS pilot project: processing, analysis of the variability and of the coupled patterns, *Ann*. *Geophys*., 20, 1-19. 2

Buongiorno Nardelli, B., Marullo, S. & Santoleri, R. (2005). Diurnal variations in AVHRR SST fields: a strategy for removing warm layer effects from daily images, *Rem*. *Sens*. *Env*., 95, 1, 47-56, doi:10.1016/j.rse.2004.12.005.

Buongiorno Nardelli B., Colella, S., Santoleri, R., Guarracino, M. & Kholod, A. (2010). A re-analysis of Black Sea Surface Temperature, *J*. *Mar*. *Sys*., 79, 1-2, 50-64, doi:10.1016/j.jmarsys.2009.07.001.

Cayula, J.-F., & Cornillon, P. (1992). Edge detection algorithm for SST images, *J*. *Atm*. *Oceanic Tech*., 9 (1), 67–80

Chao, Y., Z. Li, J. D. Farrara, and P. Huang, 2009: Blended sea surface temperatures from multiple satellites and in-situ observations for coastal oceans. *J*. *Atm*. *and Oceanic Tech*., 26 (7), 1435-1446, 10.1175/2009JTECHO592.1.

Donlon, C. J., Martin, M., Stark, J. D., Roberts-Jones, J., Fiedler, E. & Wimmer, W. (2011). The Operational Sea Surface Temperature and Sea Ice analysis (OSTIA). *Rem*. *Sens*. *Env*., doi: 10.1016/j.rse.2010.10.017 2011.

Donlon, C., J. and the GHRSST-PP Science Team (2005). The Recommended GHRSST-PP Data Processing Specification GDS (Version 1 revision 1.5). GHRSST-PP Report Number 17. Published by the *International GHRSST-PP Project Office*; UK Met Office, United Kingdom, 235 pp.

Donlon, C. J., Minnett, P. J., Gentemann, C., Nightingale, T. J., Barton, I. J., Ward, B., Murray, M. J. (2002). Toward Improved Validation of Satellite Sea Surface Skin Temperature Measurements for Climate Research, *J*. *Climate*, **15**, 353–369, doi:10.1175/1520-0442(2002)015.

Gandin, L.S. (1965). Objective analysis of meteorological fields. Israel Program for Scientific Translation, Jerusalem, pp. 242.

GHRSST Science Team, (2010). The Recommended GHRSST Data Specification (GDS) Revision 2.0 Technical Specifications, available from the *GHRSST International Project Office*, http://www.ghrsst.org, pp. 120.

Hansen, D.V. & Poulain, P.M., (1996). Quality Control and Interpolation of WOCE/TOGA drifter data. *J. Atm. Oceanic Tech.*, 13, 900-909.

Høyer, J. L., Karagali, I., Dybkjær, G. & Tonboe R. (2012). Multi sensor validation and error characteristics of Arctic satellite sea surface temperature observations, *Rem. Sens. Env.*, 121, 335-346, doi:10.1016/j.rse.2012.01.013.

Kilpatrick, K.A., Podesta, G.P., & R. Evans (2001). Overview of the NOAA/NASA Advanced Very High Resolution Radiometer Pathfinder algorithm for sea surface temperature and associated matchup database, *J. Geophys. Res*, 106 (C5): 9179-9197.

Le Borgne, P., Marsouin, A., Orain, F. & Roquet, H. (2011). Operational sea surface temperature bias adjustment using AATSR data, *Rem. Sens.. Env.*, doi: 10.1016/j.rse.2010.02.023.

Marullo S., Buongiorno Nardelli, B., Guarracino, M. & Santoleri, R. (2007). Observing The Mediterranean Sea from Space: 21 years of Pathfinder-AVHRR Sea Surface Temperatures (1985 to 2005). Re-analysis and validation, *Ocean Sci.*, 3, 299-310.

O'Carroll, A. G., Eyre, J. R. & Saunders R. W. (2008). Three way error analysis between AATSR, AMSR-E, and in situ sea surface temperature observations, *J. Atmos. Oceanic Technol.*, 25(7), 1197–1207.

Rabinovich, S. G. (2000). Measurement Errors and Uncertainties: Theory and Practice. Second Edition. Springer-Verlag, New York, ISBN-10: 0-387-25358-0, 2000.

Reynolds, R.W. (1988). A real-time global sea surface temperature analysis. *J. Climate*, 1, 75-86.

Reynolds, R. W., Rayner, N. A., Smith, T. M., Stokes D. C., & Wang, W. (2002). An improved in situ and satellite SST analysis for climate. *J. Climate*, **15**, 1609-1625.

Reynolds, R. W., Smith, T. M., Liu, C., Chelton, D. B., Casey, K. S. & Schlax, M. G. (2007). Daily high-resolution blended analyses for sea surface temperature. *J. Climate*, 20, 5473- 5496.

Reynolds, R. W., & Chelton, D. B. (2010). Comparisons of daily sea surface temperature analyses for 2007-08. *J. Climate*, 23.

Sakaida, F., Takahashi, S., Shimada, T., Kawai, Y., Kawamura, H., Hosoda, K. & Lei Guan, K. (2005). The production of the new generation sea surface temperature (NGSST-O ver.1.0) in Tohoku University, *Geoscience and Remote Sensing Symposium*. IGARSS '05. Proceedings IEEE International, 25-29 July 2005, Vol.4, 2602-2605, ISBN:0-7803-9050-4, doi:10.1109/IGARSS.2005.1525518 .

660 Santoleri, R., Marullo, S., & Böhm, E. (1991). An objective analysis scheme for AVHRR imagery,
661 *Int*. *J*. *Rem*. *Sens*., 12, 4, 681-693.
662 Xu, F., & Ignatov, A. (2010). Evaluation of in situ SSTs for use in the calibration and validation of
663 satellite retrievals. *J*. *Geophys*. *Res*., 115, C09022, doi:10.1029/2010JC006129.
664

## FIGURES & TABLES

Table 1. Hierarchy of the L2P data used as input to the MyOcean ISAC-GOS HR SST chain (2010-2011).

| | L2P code | Sensor | Platform | Res. |
|---|---|---|---|---|
| **1** | ATS_NR_2P | AATSR | ENVISAT/POLAR | 1 km |
| **2** | AVHRR_METOP_A | AVHRR | METOP_A /POLAR | 1 km |
| **3** | NAR18_SST | AVHRR | NOAA-18 /POLAR | 2 km |
| **4** | MODIS_T | MODIS | TERRA /POLAR | 1 km |
| **5** | NAR17_SST | AVHRR | NOAA-17 /POLAR | 2 km |
| **6** | MODIS_A | MODIS | AQUA /POLAR | 1 km |
| **7** | SEVIRI_SST | SEVIRI | MSG/GEOSTATIONARY | 0.1° |

Table 2. OI parameters used in MyOcean ISAC-GOS SST chain

| OI PARAMETERS | HR (0.0625°) | UHR (0.01°) |
|---|---|---|
| SPATIAL DECORRELATION SCALE | 150 km | 5 km |
| TEMPORAL DECORRELATION SCALE | 7 days | 1 day |
| NOISE-TO-SIGNAL RATIO | 0.3 | 0.5 |
| FIRST GUESS FIELD | HR pentad climatology | upsized HR L4 |
| SPATIAL INFLUENTIAL RADIUS | 300-900 km | 20 km |
| TEMPORAL WINDOW | ±10 DAYS (NRT=-10) | ±2 DAYS (NRT=-2) |

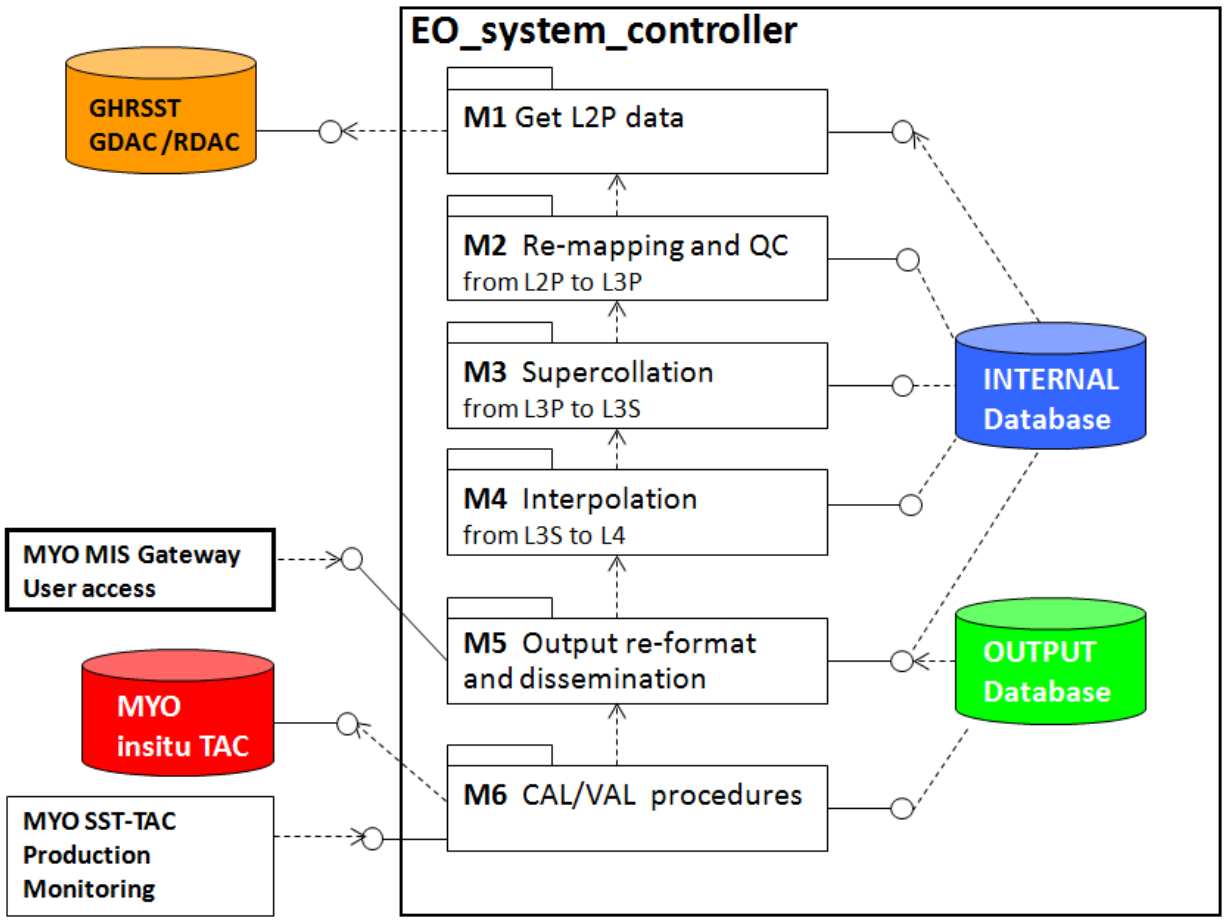


676

677

678 Fig.1 Scheme of the L4 SST processing chain designed by ISAC-GOS in the framework of MyOcean SST-TAC.

679 Arrows indicate dependencies, while circles represent interfaces.

680

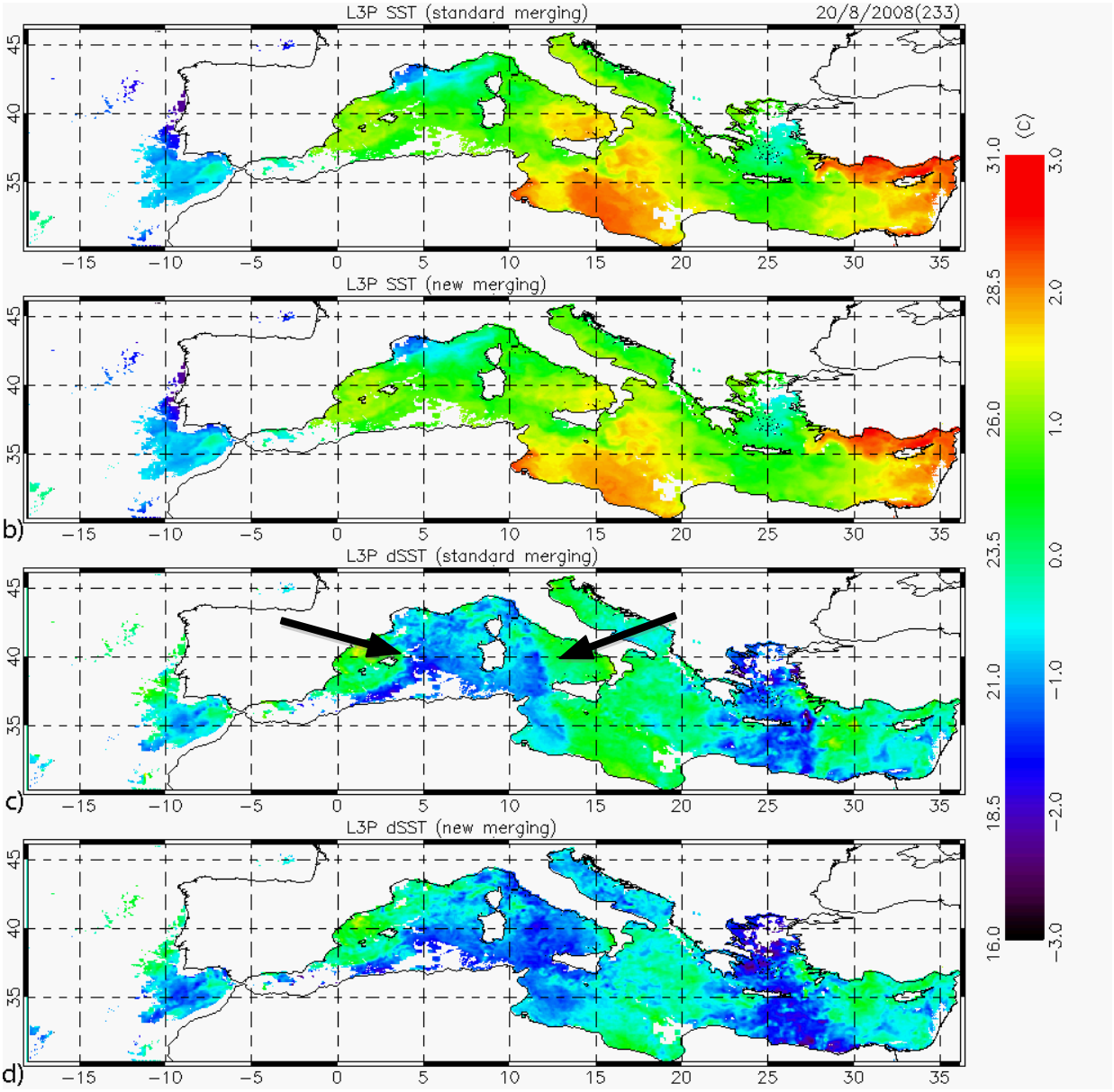


Fig.2 Example of SST (a,b) and ΔSST (c,d) fields obtained with the preliminary (a,c) and advanced (b,d) supercollating algorithms.

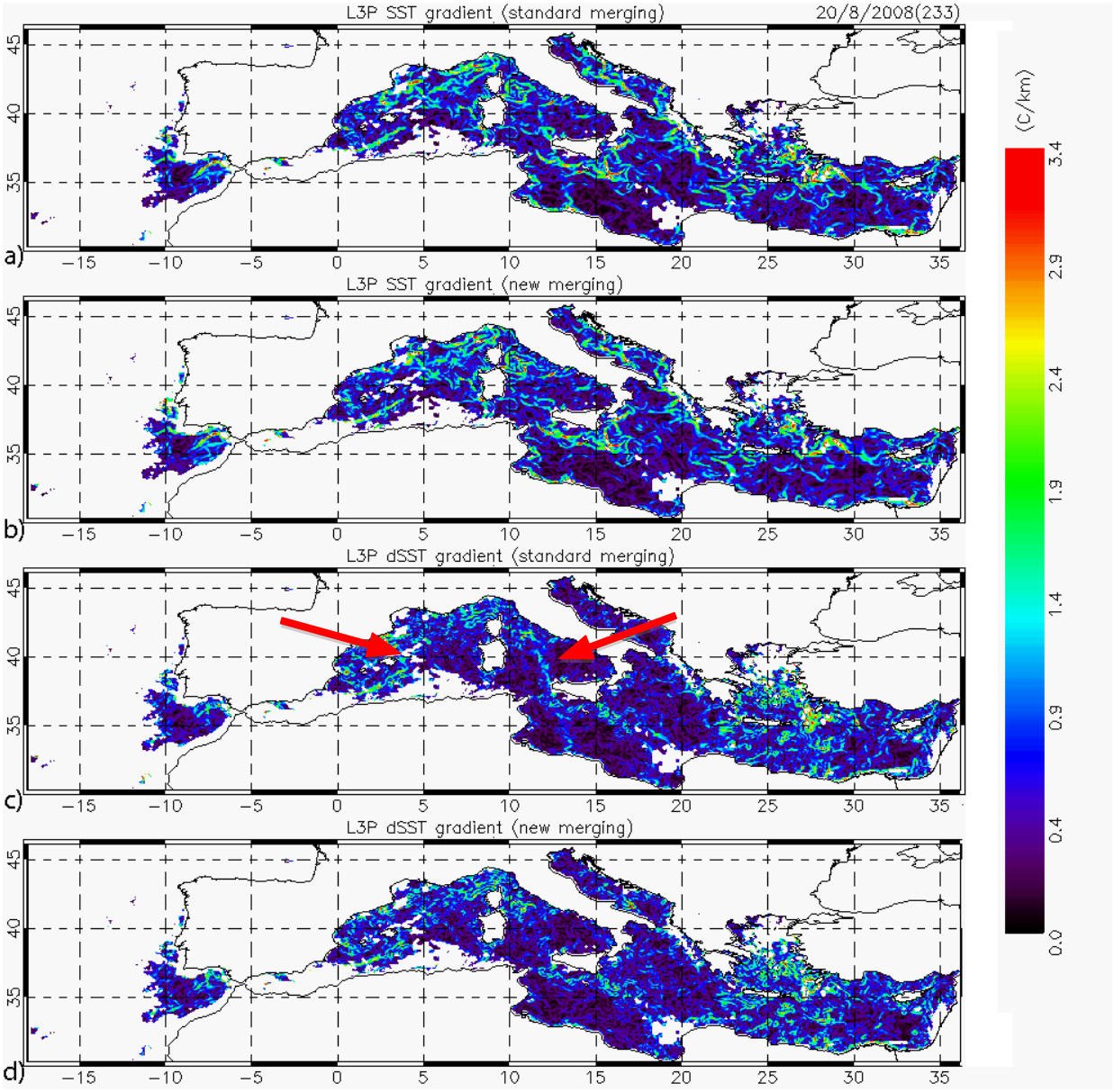


684

685 Fig.3 Example of SST gradient (a,b) and ΔSST gradient (c,d) fields estimated from the preliminary (a,c) and advanced

686 (b,d) supercollated L3data.

687

688

689

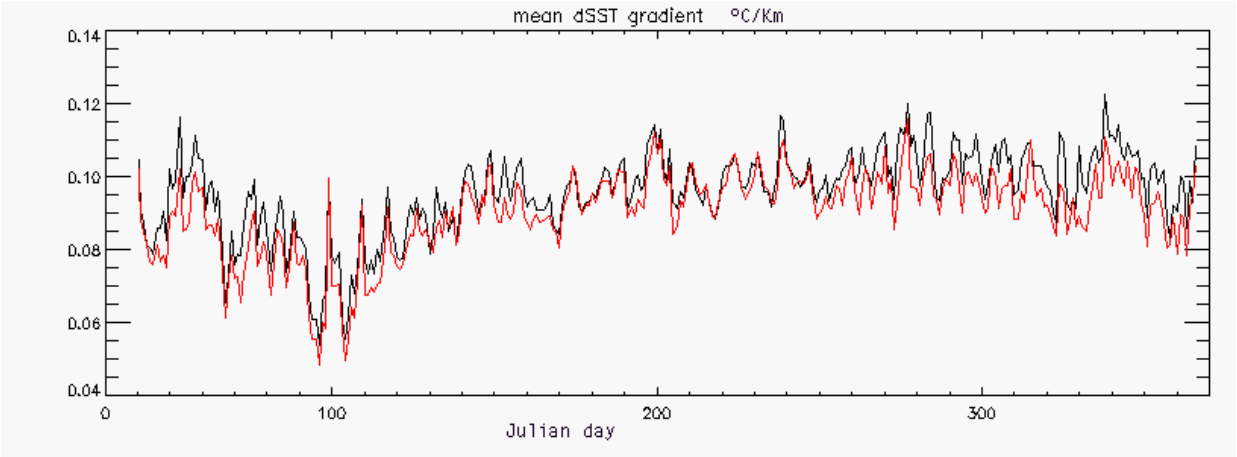


690

691 Fig.4. Spatially averaged ΔSST gradient estimated from ISAC-GOS 2008 Mediterranean supercollated L3 products

692 obtained from the V1 (black) and V2 (red) merging algorithms.

693

694

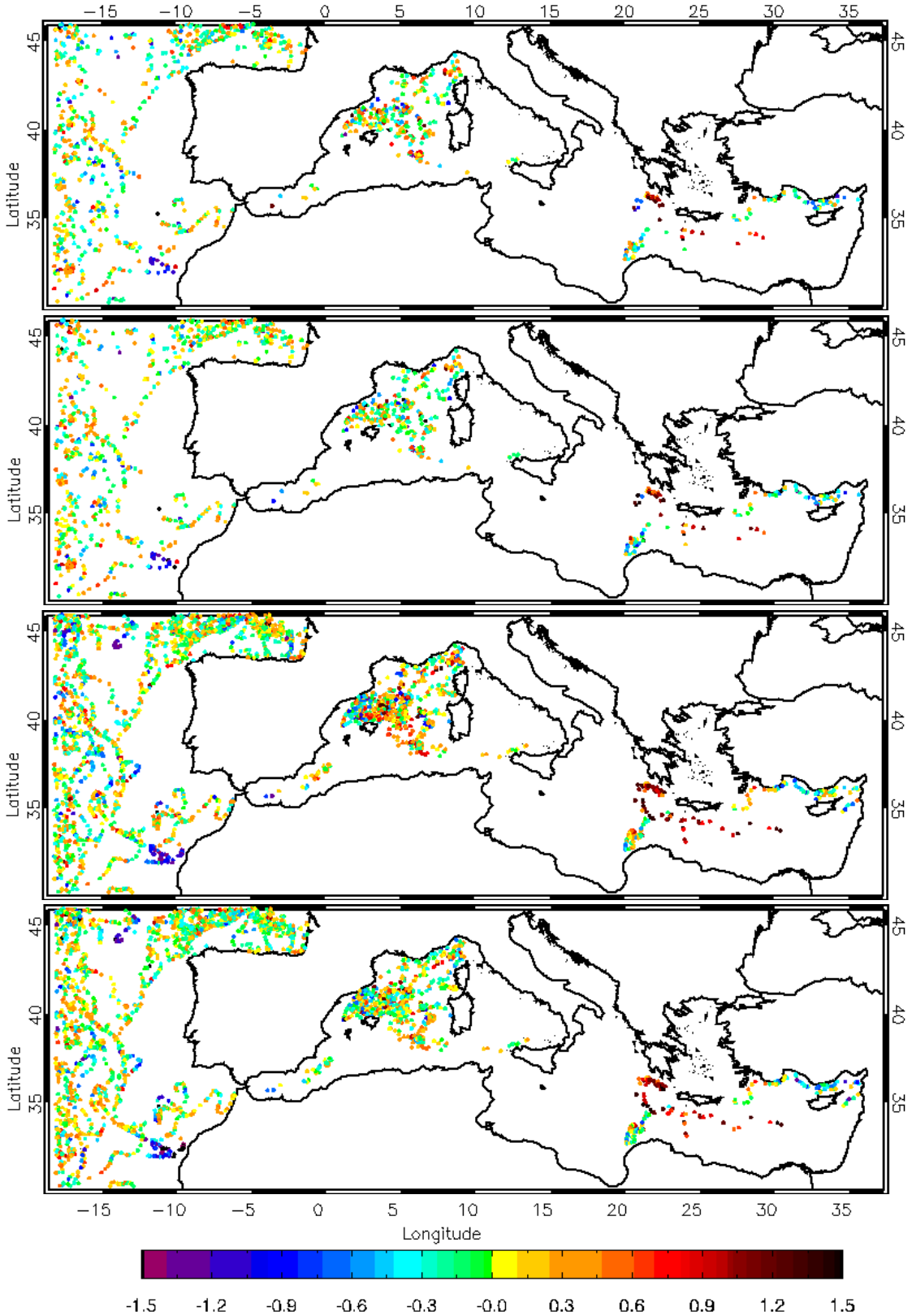


Fig. 5. Spatial distribution of the 2008 satellite/in situ match-ups and associated SST difference found with the two different super-collating algorithms considered: V1 HR L3S (a), V2 HR L3S (b), V1 HR L4 (c), V2 HR L4 (d).

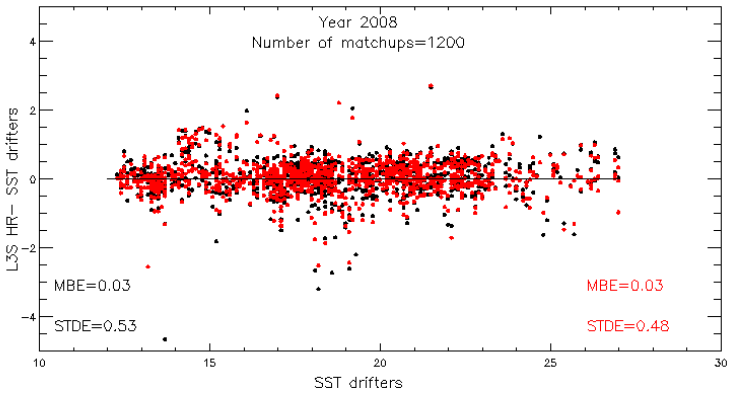


a)

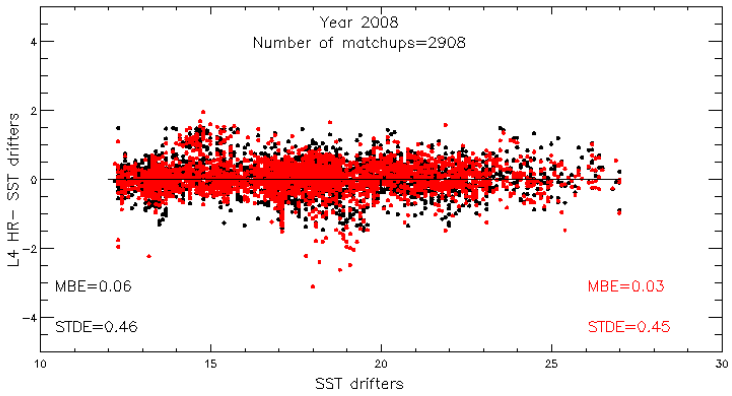


b)

Figure 6. Satellite/in situ SST differences as a function of the in situ SST. The differences are computed between the V1 supercollated satellite SST L3 (a), the corresponding V1 SST L4 (b) and in situ drifting buoy measurements (black dots), and between the V2 supercollated satellite SST L3 (a), the corresponding SST L4 (b) and in situ drifting buoy measurements (red dots).

720 a)

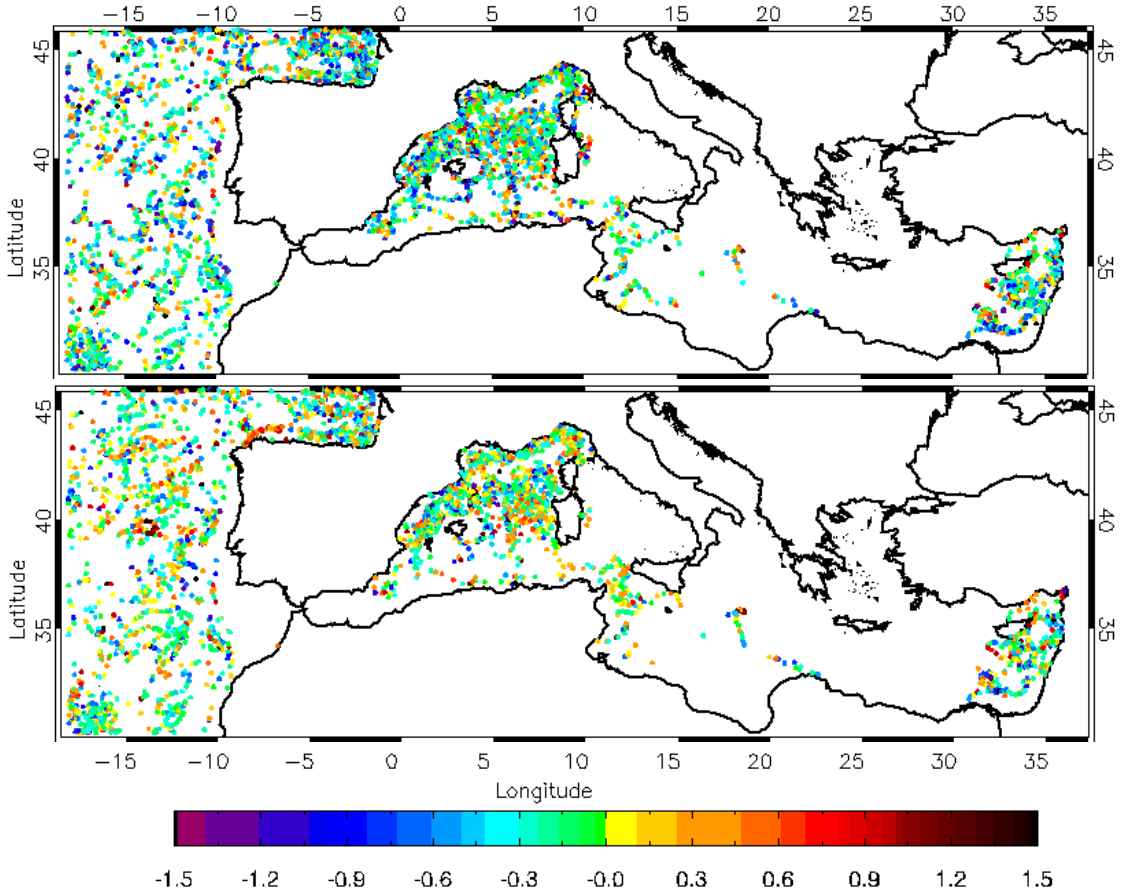


721 b)

722
723

724 Figure 7. Spatial distribution of the satellite/in situ match-ups and associated SST difference for the HR L3S (a) and

725 UHR L3S (b) during the years 2010-2011.

726

727 a)

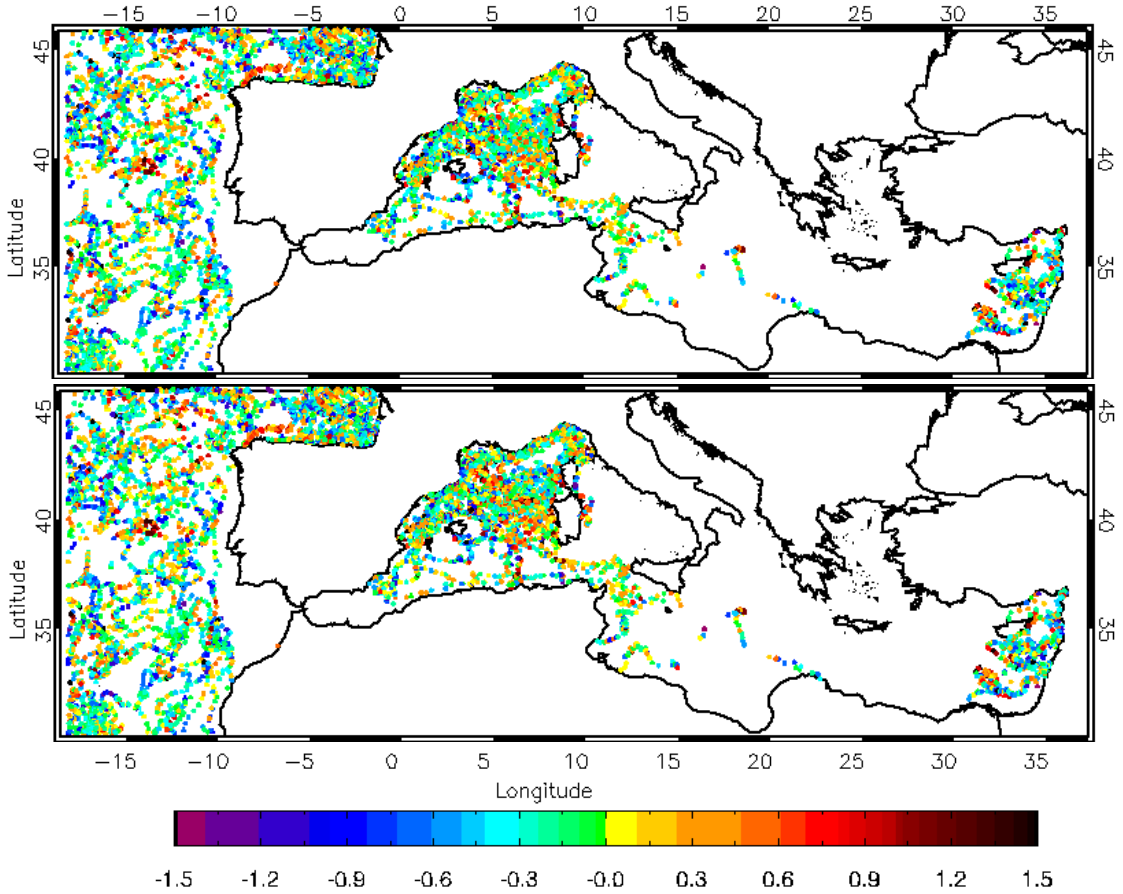


728 b)

729
730

731 Figure 8. Spatial distribution of the satellite/in situ match-ups and associated SST difference for the HR L4 (a) and

732 UHR L4 (b) during the years 2010-2011.

733

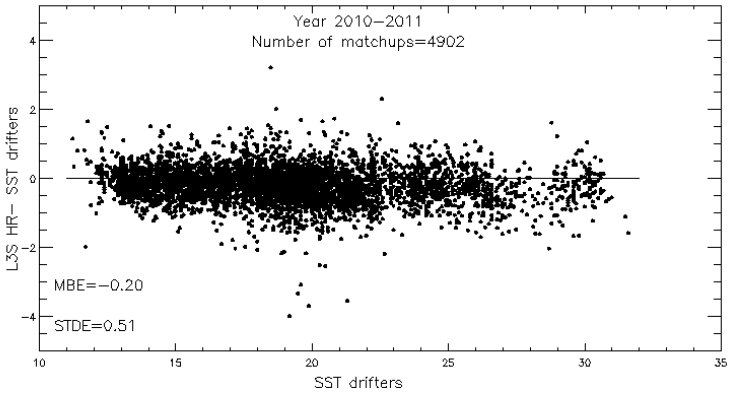


a)

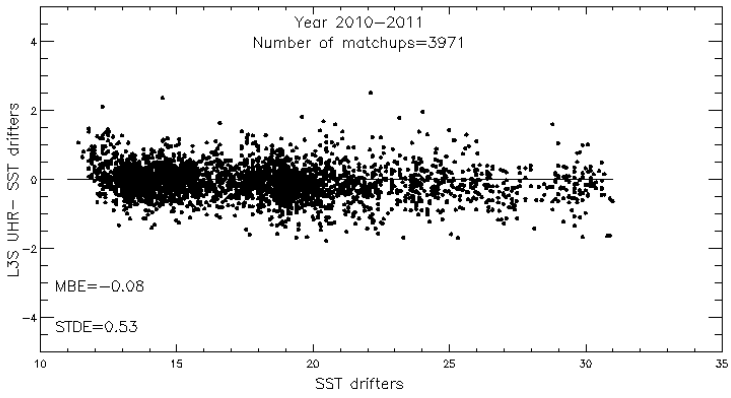


b)

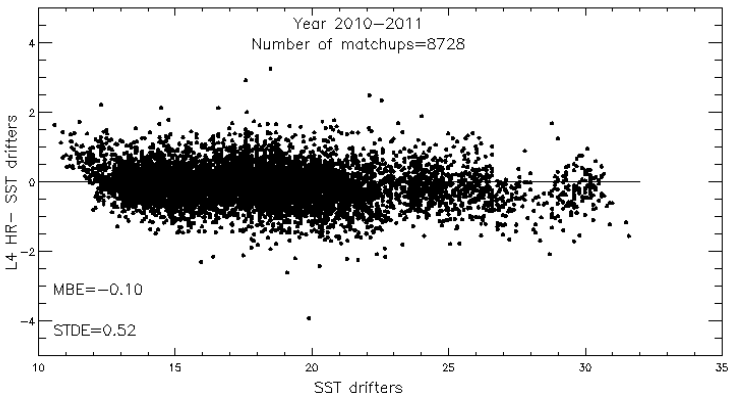


c)

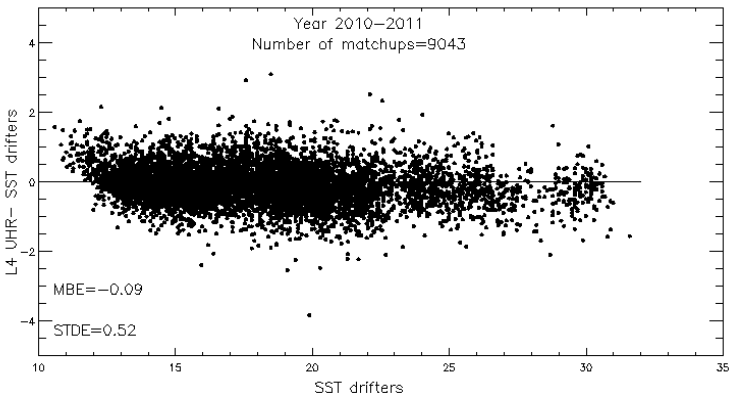


d)

Figure 9. Satellite/in situ SST differences as a function of the in situ SST. The differences are computed between the HR and UHR L3S (a,b), HR and UHR L4 (c,d) and in situ drifting buoy measurements covering the years 2010-2011.

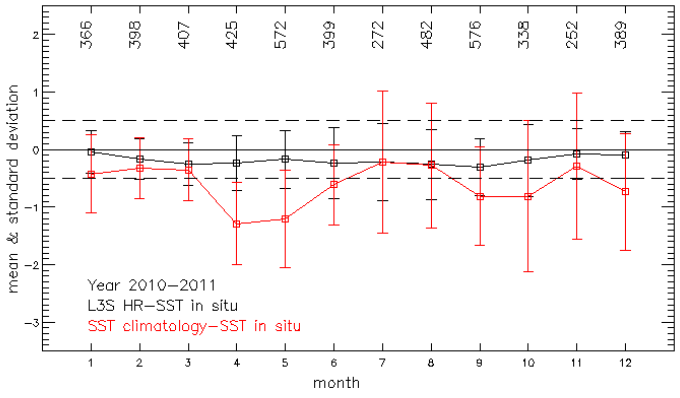


741 a)

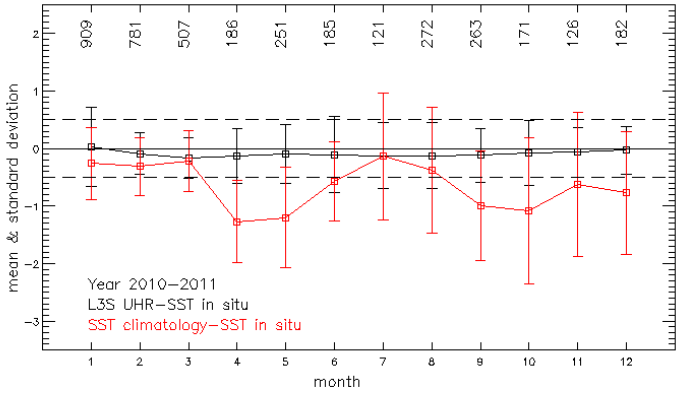


742 b)

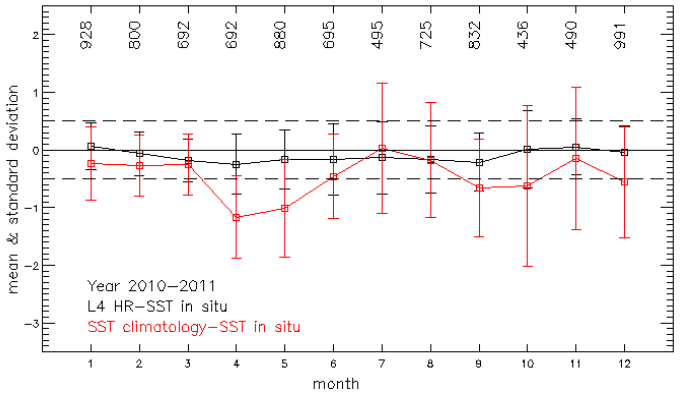


743 c)

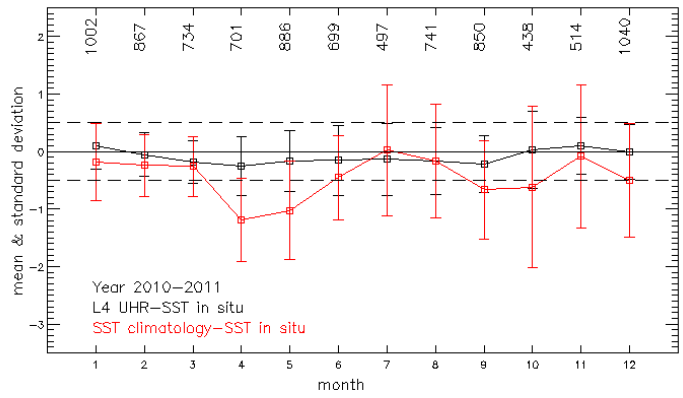


744 d)

745 Figure 10. Monthly statistics (mean bias and standard deviation error) of the difference between HR L3S (a), UHR L3S

746 (a), HR L4 (c), UHR L4 (d) and in situ data (black dots) (period 2010-2011). In red, the mean bias between the

747 corresponding pentad climatology the in situ data. The number of matchups used to estimate the values is indicated in
748 the upper part of the plot.
749